International Journal of Heat and Mass Transfer 193 (2022) 122961

Contents lists available at ScienceDirect

International Journal of Heat and Mass Transfer

journal homepage: www.elsevier.com/locate/hmt

Design and optimization on symmetrical wing longitudinal swirl generators in circular tube for laminar flow

Yongji Wang, Peng Liu, Hui Xiao, Zhichun Liu, Wei Liu*

School of Energy and Power Engineering, Huazhong University of Science and Technology, Wuhan 430074, China

ARTICLE INFO

Article history:
Received 5 January 2022
Revised 6 April 2022
Accepted 21 April 2022

Keywords:
Swirl generators
Thermal hydraulic performance
Exergy destruction minimization
Multiple longitudinal swirling flows
Multi-objective optimization

ABSTRACT

It is crucial to further improve the overall performance of heat exchanger tube and make it adapt to higher flux conditions. In this paper, a novel type of tube inserts, symmetrical wing longitudinal swirl generators (SWLSGs), was proposed and its thermal hydraulic performance was numerically investigated under laminar flow. The effect of four geometrical parameters (inclined angle (φ_1), face angle (φ_2), wing angle (φ_3) and pitch (P)) was explored. The results showed the mechanisms of heat transfer augmentation for SWLSGs could be divided into two main categories. The first one was that a longitudinal swirl flow with multi-vortexes would be formed by symmetrical wings. The other one was that SWLSGs had a structure similar to a deflector, which guided the cold water in the center to scour tube wall. This study found that the variation ranges of Nu/Nu_0, f/f_0, and the efficiency evaluation criterion (EEC) were 5.00–10.22, 4.05–14.20, and 0.71–1.35, respectively. Both exergy destruction of heat transfer and fluid flow increased as face angle and wing angle increased, and decreased as inclined angle and pitch increased. Exergy destruction minimization principle was adopted to optimize SWLSGs. After fitting function through artificial neural network, genetic algorithm was applied to obtain the Pareto front. The physical parameters of the compromised point on the Pareto front were φ_1=25.6°, φ_2=142.0°, φ_3=13.4°, P = 64.7 mm, and EEC = 1.26. The EEC of the highest point of the ratio of the exergy destruction of heat transfer and fluid flow ($REHF$) was 1.48. The present work provided a new method for multi-parameter study of tube inserts, and proved that the exergy destruction as evaluation was an effective evaluation index for design and optimization.

1. Introduction

As an important equipment of heat and mass transfer, heat exchanger tubes have been proverbially used in refrigerating, manufacturing and metallurgy systems. In the field of modern industry, there is an inevitable process of heat conversion and management. It is of utmost importance to improve heat exchanger thermal hydraulic performance for energy utilization. Under fixed magnitude of heat transfer, the goal of heat transfer augmentation is to reduce the volume of the heat exchanger, and also to reduce power consumption as much as possible. Techniques of heat transfer augmentation mainly contain active and passive ones. Active techniques require extra pump power for the heat system, which increase the complexity of the system. Passive techniques [1] refer to modifying the heat transfer surface or adding displayed enhancement devices to the fluid. Modification of heat transfer surface and change of cross-sectional area are mainly applied to turbulent state, such as internally grooved tubes [2] and twisted oval tubes [3] and so on. Whereas, tube inserts can effectively enhance convective heat transfer under laminar flow. Tube inserts have been widely used because of their advantages of simple systems, easy to install and disassemble. Currently, there are various types of tube inserts, which could be simply divided into twisted tapes, coiled wires, vortex generators, porous media, etc. The primary purpose of tube inserts was heat transfer augmentation, but the large increase in pressure drop overwhelmed the thermal system. Excessive pump power consumption would bring about a higher cost and limit the application of heat transfer augmentation techniques. Therefore, it was particularly significant to weigh the benefits of heat transfer augmentation and the costs of power consumption.

Twisted tapes are able to generate strong secondary flow. Researchers improved the classic twisted tapes and proposed hollow twisted tapes [4], helically twisted tapes [5], twisted tapes with structure like ribs [6] and others [7]. Zhang et al. [8] applied the principle of multi-field synergy to illustrate the mechanism of heat transfer augmentation in circular tubes with multiple regularly spaced twisted tapes. With the increase of the number of twisted tapes, the increase times of the friction factor was larger

* Corresponding author.
E-mail address: w_liu@hust.edu.cn (W. Liu).

https://doi.org/10.1016/j.ijheatmasstransfer.2022.122961
0017-9310/

Nomenclature

a	the length of the inlet section
ANN	artificial neural network
b	thickness of the connection with center rod
c_p	specific heat capacity
d	diameter of center rod
D	inner diameter of tube
EEC	efficiency evaluation coefficient
$E_{xd,\Delta T}$	heat transfer exergy destruction
$E_{xd,\Delta p}$	flow exergy destruction
f	friction factor
h	enthalpy
h_r	radial dimension of the insert
h_m	average heat transfer coefficient
L	length of the tube
MSE	mean square error
NSGA	non-dominated sorting genetic algorithm
Nu	Nusselt number
P	pitch of the insert
Δp	pressure drop
R	transitional radius
Reg	Regression coefficient
Re	Reynolds number
t	thickness of the insert
T	temperature

Subscripts

0	smooth tube
in	tube inlet
w	tube wall
m	average
c	equivalent value in smooth tubes

Greek symbols

λ	thermal conductivity of water
ρ	density of water
μ	dynamic viscosity of water
φ_1	inclined angle of the insert
φ_2	face angle of the insert
φ_3	wing angle of the insert

than that of Nusselt number. Furthermore, heat transfer performance would be further improved by adding fins or ribs to the traditional twisted tapes, so researchers had made a lot of improvements on the basic tapes. Eiamsa-ard et al. [9] studied on thermal hydraulic performance in circle tube fitted with delta-winglet twisted tapes (DWT). They found *Nu* number and *f* of DWT were higher than those of classical twisted tapes, and DWT had better heat transfer enhancement and could effectively dwindle the size of heat exchanger.

Coiled wires [10,11] form a swirl flow in tube, which increase the flow path and mean retention time of the fluid, thus achieving the purpose of heat transfer augmentation. Feng et al. [12] studied the rectangular microchannel heat sink with helical coils, and the results showed that longitudinal swirl flow in the microchannel was generated. The study found that flow resistance also increased while the heat transfer performance was improved. Promvonge [13] numerically investigated the coiled square and round wires in circular tubes. And they found the heat transfer performance with coiled square wires was stronger than that of the round cross section.

Vortex generators will produce swirl flow, which are widely used to strengthen fluid mixing and local turbulence for heat transfer augmentation. Deshmukh and Vedula [14] proposed curved delta wing vortex generators, and thermal hydraulic performance was experimentally studied under turbulent flow with air as working medium. Deshmukh et al. [15] removed the steel pin which curved delta wing attached and experimentally investigated this insert with water as working medium under laminar flow. In both turbulent and laminar flow states, curved delta wing vortex generators deflected the mainstream fluid to create tangential velocity to scour the tube wall and had higher local Nusselt number than other coiled wires. However, vortex generators also have disadvantages. There are local reverse flow and eddy behind vortex generators resulting in fluid momentum loss and flow dead zone.

In order to reduce local reverse flow and eddy so as to better organize fluid flow and heat management, an optimal flow field structure with low power consumption must be proposed. Chen et al. [16] and Liu et al. [17,18] conducted heat transfer and flow dissipation minimization as optimal goals and created a mathematical model for thermal optimization based on variation principle. They both obtained the low-dissipation flow field with the structure of 'multiple longitudinal swirling flow'. The longitudinal swirl generators effectively reduce reverse flow and enhance convective heat transfer while reducing flow power consumption. Subsequently, many scholars proposed various longitudinal swirl generators [19–22]. Zheng et al. [23] carried out a numerical analysis on heat transfer and power consumption of the tube fitted with a vortex rod insert. They found that the vortex rod generated longitudinal swirl flow in the tube. And they investigated the effect of pitch and ratio of rod length. Liu et al. [24] came up with a bidirectional conical strip insert, mixing cold and heated water effectively between core flow and boundary flow. The bidirectional conical strip inserts suppressed the formation of local eddy and effectively reduced the flow resistance. Lv et al. [25] numerically investigated a circular tube inserted by center-connected deflectors that guided the fluid to scour the boundary region. The increase of wall temperature gradient would strengthen the convective heat transfer.

The existing theories and principles of heat transfer enhancement provide guidance for thermal design techniques. Bejan [26,27] developed the entropy analysis method existed in thermodynamics into the process of convective heat transfer, proposing entropy generation minimization principle. Entropy generation quantificationally describes the irreversibility of heat transfer and could be the indicator to measure the quality of thermal system. Guo et al. [28,29] came up with the physical concept of entransy to describe the ability of heat transfer. They illustrated the principle of entransy dissipation extreme for analyzing heat transfer characteristics. Liu et al. [17,30] came up with available potential *e* to describe the heat transfer capacity of working medium. They developed the exergy destruction minimization principle by taking the unavailable heat below ambient temperature of convection process into account. Entropy generation, entransy dissipation and exergy destruction were mathematical descriptions of the convective irreversibility, representing the irreversibility of heat transfer process. Therein, exergy destruction also included the loss of mechanical energy of fluid, representing the irreversibility of fluid flow. Therefore, exergy destruction analysis method derived from available potential described the convective heat transfer process more comprehensively from two aspects of irreversibility of heat transfer and flow.

As mentioned above, multi-vortexes would improve the temperature uniformity in tubes with moderate increase of pressure drop. In order to enhance heat transfer performance and reduce the friction factor at the same time, the symmetrical wing longitudinal swirl generators was proposed in this paper. Based on literature research, we selected the factors that significantly affect the thermal hydraulic performance, and the effect of four geometrical parameters of SWLSGs (inclined angle (φ_1), face angle (φ_2), wing

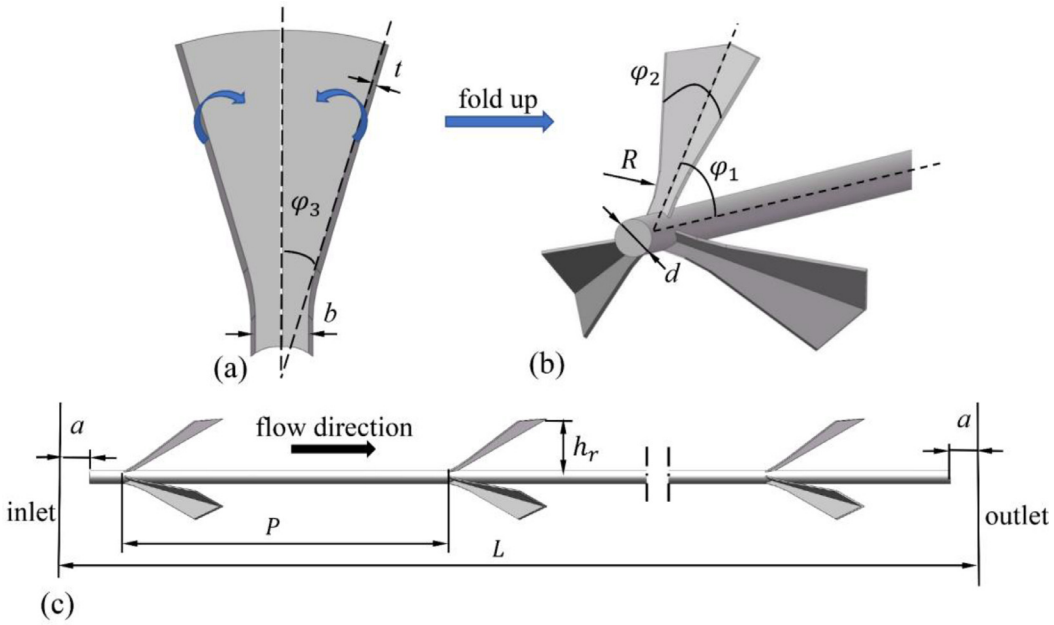

Fig. 1. Geometrical model of the enhanced tube: (a) a wing; (b) center-connected symmetrical wings; (c) the position of SWLSGs.

Table 1
Geometrical parameters of SWLSGs.

D /(mm)	L /(mm)	d /(mm)	a /(mm)	h_r /(mm)	R_t /(mm)
20	500	2	5	9	10
t /(mm)	b /(mm)	φ_1 /(°)	φ_2 /(°)	φ_3 /(°)	P /(mm)
0.2	0.8	20,30,40,50,60	90,110,130,150,170	10,12.5,15,17.5,20	40,50,60,70,80

angle (φ_3) and pitch (P)) was explored. Exergy destruction analysis method was adopted in this paper. And we apply neural network fitting [31] and Non-dominated sorting genetic algorithm-II(NAGS-II) [32,33] to optimize SWLSGs.

2. Geometrical model description

In numerous engineering systems, convective heat transfer exists between the wall and fluid. The key of convective heat transfer augmentation was to improve temperature uniformity, temperature gradient near the wall and reduce pressure drop in the fluid domain. Fig. 1 showed the geometrical model of an enhanced tube inserted symmetrical wing longitudinal swirl generators (SWLSGs). These four parameters, such as inclined angle (φ_1), face angle (φ_2), wing angle (φ_3) and pitch (P), were numerically investigated in this paper. The inner diameter and length of the circle tube (L) were 20 mm and 500 mm, respectively. And the number of symmetrical wings was two or less could not guarantee sufficient mixing of the fluid. Therefore, the number of symmetrical wings in the circumferential direction was constant of 3. The geometric parameters of SWLSGs were as follows: the transition radius (R_t) was 10 mm; the length of the inlet and outlet section (a) were both 5 mm; the radial height (h_r) was constant at 9 mm, the thickness (t) of symmetrical wings was constant of 0.2 mm. Five different values of pitch (P), inclined angle (φ_1), face angle (φ_2) and wing angle (φ_3) were selected for numerical calculation. These parameters were listed in Table 1.

Since there are four factors and each with five levels each, a large amount of computing resources would be occupied if a full-scale test was carried out. Orthogonal design of experiment was a method for studying problems with multi-factors and multi-levels. It had the characteristics of balanced parameter distribution, high efficiency and economy. According to the orthogonal table, several representative examples were selected to carry out the experiment at the cost of missing some examples. Without considering the interaction between factors, the orthogonal table of $L_{25}5^6$ was selected, the factors were arranged in the first four columns of the table, and the number of tests was 25. Due to the characteristics of the orthogonal table, at least three parameters of any two tests were different.

3. Numerical simulation

3.1. Governing equations and boundary conditions

In this paper, water is chosen as the working medium. The Reynolds number is selected as 300–1500 for laminar flow. Because the range of temperature is limited, the properties of fluid are constant, ignoring the effect of radiation. And the enhanced tube is placed horizontally, ignoring the effect of gravity. The governing equations of mass, momentum and energy conservation are applied.

$$\frac{\partial u_i}{\partial x_i} = 0 \tag{1}$$

$$\frac{\partial}{\partial x_j}\left(\rho u_i u_j\right) = -\frac{\partial p}{\partial x_i} + \frac{\partial}{\partial x_j}\left[\mu\left(\frac{\partial u_i}{\partial x_j} + \frac{\partial u_j}{\partial x_i}\right)\right] \tag{2}$$

$$\frac{\partial}{\partial x_i}\left(\rho u_i c_p T - \lambda \frac{\partial T}{\partial x_i}\right) = 0, (i, j = 1, 2, 3) \tag{3}$$

where u_i is the velocity component in the direction of x_i, ρ is the density of water, μ is the dynamic viscosity, c_p is the specific heat capacity, and λ is the thermal conductivity.

All the simulations are carried out by using the commercial CFD software Fluent 19.0, based on the finite volume method. Outflow boundary condition is applied at the outlet. The boundary

conditions of the tube wall are no slip and constant heat flux 2000 W/m². The fully developed temperature and velocity boundary conditions are applied at the inlet.

SIMPLE algorithm is selected for coupling pressure and velocity. Pressure, momentum and energy equations are solved with a second-order upwind discrete format. The residuals of continuity and momentum equations are set as 10^{-6}, and the residuals of energy equations are set as 10^{-8}.

3.2. Data acquisition

The Reynolds number (Re):

$$Re = \frac{\rho u_m D}{\mu} \tag{4}$$

where u_m is the average velocity.

Average heat transfer coefficient in the tube h_m:

$$h_m = \frac{q}{T_w - T_m} \tag{5}$$

where T_w is the average temperature of the tube wall; T_m is the average temperature of the fluid.

The calculation formula of Nusselt number (Nu) and the resistance coefficient f in the tube are as followed:

$$Nu = \frac{h_m D}{\lambda} \tag{6}$$

$$f = \frac{\Delta p}{\left(1/2\rho u_m{}^2\right)(x/D)} \tag{7}$$

where Δp and x are the pressure drop and length of the selected tube segment.

For an incompressible fluid in a steady fluid dynamics system, $\partial p/\partial t = 0$. So the total derivative of the available potential for incompressible fluid can be expressed as [30],

$$\rho\frac{De}{Dt} = -\nabla\cdot\left[\left(1-\frac{T_0}{T}\right)\boldsymbol{q}\right] + \left(1-\frac{T_0}{T}\right)\Phi - T_0\frac{\lambda(\nabla T)^2}{T^2} - \boldsymbol{U}\cdot\left(\rho\boldsymbol{U}\cdot\nabla\boldsymbol{U} - \mu\nabla^2\boldsymbol{U}\right) \tag{8}$$

The first item on the right of the equation is the total exergy flux into the system. The second term is the viscous dissipation, which is so small in calculation that it could be ignored. The remaining two terms are local exergy destruction in the process of convective heat transfer, where $T_0\frac{\lambda(\nabla T)^2}{T^2}$ is unavailable heat below ambient temperature, so reducing the temperature gradience in thermal process will reduce the exergy destruction of heat transfer. The last item $\boldsymbol{U}\cdot(\rho U\cdot\nabla U - \mu\nabla^2 U)$ is the exergy destruction of fluid flow owing to the pressure drop. The principle of exergy destruction minimization is to minimize partial exergy destruction, achieving high efficiency of energy conversion. Exergy destruction of heat transfer and fluid flow are caused by temperature difference and pressure drop, respectively,

$$E_{xd,\Delta T} = \iiint_\Omega T_0\frac{\lambda(\nabla T)^2}{T^2}dV \tag{9}$$

$$E_{xd,\Delta p} = \iiint_\Omega \boldsymbol{U}\cdot\left(\rho\boldsymbol{U}\cdot\nabla\boldsymbol{U} - \mu\nabla^2\boldsymbol{U}\right)dV \tag{10}$$

The efficiency evaluation criterion (EEC) is defined as:

$$EEC = \frac{Q/Q_0}{P_W/P_{W0}} = \frac{Q/Q_0}{\Delta P/\Delta P_0} = \frac{Nu/N_{u0}}{f/f_0} \tag{11}$$

where subscript 0 represents the smooth circular tube. Q represents heat fluxes; P_w represents power consumptions, P_w can be replaced by pressure drop Δp when the Reynolds number of tubes is the same. According to the formula of resistance coefficient and pressure drop in circular tubes, $EEC = (Nu/Nu_0)/(f/f_0)$ is finally obtained. The characteristic of EEC is the ratio of the benefit of heat transfer augmentation to the cost of power consumption. EEC attaches equal importance to heat transfer augmentation and power consumption increase, which can directly evaluate whether it is profitable to enhance the overall heat transfer performance of the enhanced tubes. $EEC > 1$ means profitable. The larger EEC means that the heat transfer benefit exceeds more obviously power consumption augmentation.

Table 2
Grid independence test.

Grid system	Grid number	Nu	Relative error-Nu	f	Relative error-f
1	4,759,056	33.675	3.41%	0.49252	1.09%
2	7,046,782	34.773	0.26%	0.49482	0.62%
3	14,709,596	34.865	–	0.49793	–

Table 3
The range analysis.

Test index	The impact from high to low
Nu	φ_1 P φ_3 φ_2
f	φ_3 P φ_2 φ_1
EEC	φ_3 φ_2 P φ_1

3.3. Mesh system and validation of numerical model

As shown in Fig. 2, ICEM 19.0 was applied to generate the hybrid unstructured grids, including tetrahedron, hexahedron, prism and pyramid grids in the numerical simulation. Mesh near the tube wall and insert surface was used to accurately capture the detail of thermal hydraulic characteristics. Three grid systems (4,759,056, 7,046,782 and 14,709,596 elements, respectively), were generated for Case2 (φ_1=20°, φ_2=110°, φ_3=15° and P = 70 mm). As can be seen from the Table 2, the relative errors of Nu and f were 0.26% and 0.62%, respectively. This indicates that grid system 2 had already met the requirements of modulated precision. Therefore, grid system 2 was applied for numerical simulation.

As shown in Fig. 3, in order to verify the credibility of laminar flow in smooth tubes, the simulated results of Nu number and f were compared with those from the theoretical formulas. The inlet boundary conditions were fully developed temperature and velocity, so the theoretical formulas in circular tubes under laminar flow (Re<2100) were Nu_0 = 4.36 and f = 64/Re [34]. The maximum relative errors of Nu number and f were 3.47% and 2.66%. For verifying the accuracy of the numerical simulation of the enhanced tube, the results of numerical method in this paper were compared with the experiment results [15]. The geometrical structure in the experiment was modeled and calculated. As shown in Fig. 4, the maximum relative errors of Nu number and f were 8.21% and 9.37%, respectively. The uncertainty of the experiment measurement: Nusselt number was about 14.4% and the friction coefficient was about 10.3%, so the numerical method in this work was feasible and convincing.

4. Results and discussion

4.1. Results of orthogonal design of experiment

The heat transfer in the fully developed section is increased by 5.00–10.22 times, the friction factor is increased by 4.19–14.20 times, and the range of EEC is 0.71–1.26. The range analysis is applied on the four factors, and the factors are ranked from highest to lowest in order of the magnitude of their impact, as shown in Table 3. The inclined angle φ_1 has the greatest influence on Nusselt number, so the best way to improve Nu is to reduce the inclined

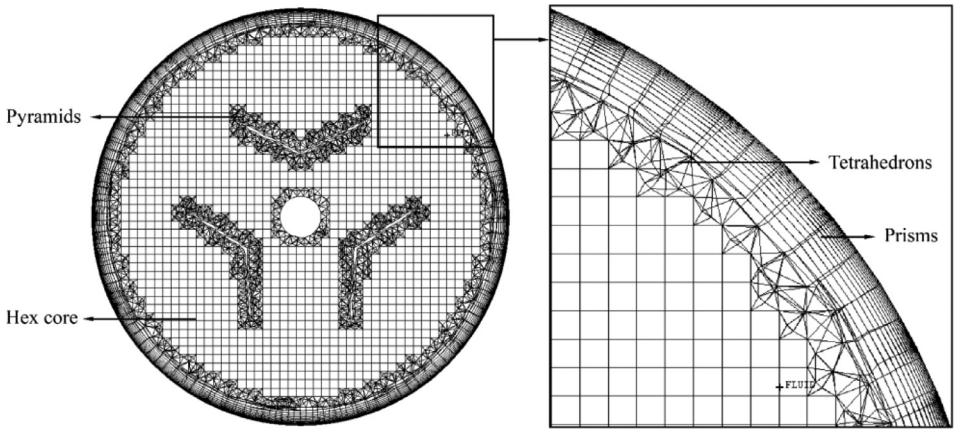

Fig. 2. Mesh generation in computational domain.

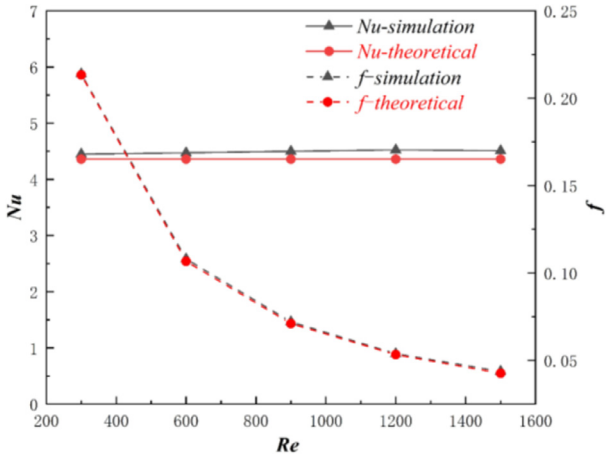

Fig. 3. Numerical simulation verification of smooth tube.

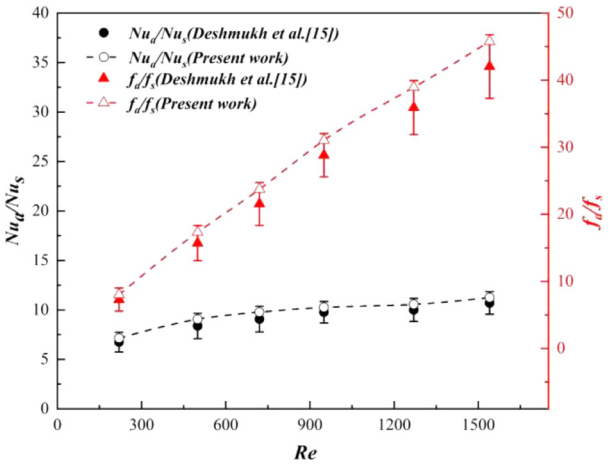

Fig. 4. Numerical simulation and experimental [15] verification of the enhanced tube.

angle. The wing angle φ_3 has the greatest influence on friction factor and *EEC*. When friction factor is smaller, the *EEC* is larger, so it can be summarized simply as that *EEC* is more sensitive to flow dissipation reduction. Therefore, for improving the overall performance of the enhanced tube, the friction factor should be reduced as much as possible while ensuring adequate heat transfer augmentation.

4.2. Heat transfer and flow characteristics

The temperature of water in the enhanced tube is more uniform due to disturbance effects of SWLSGs. As shown in Figs. 5 and 6(a), there are two main mechanisms of heat transfer augmentation. As shown in Fig. 5(a), the first one is that symmetrical wings with circular array distribution can be used as longitudinal swirl generators to form multi-vortexes in the tube. Each pair of vortexes acts on the mixing of the heated water in boundary flow and the cold water in core flow, leading to a more homogeneous temperature profile. As the temperature difference of the fluid is reduced, exergy destruction of heat transfer will decrease according to Eq. (9), which means less irreversibility and unavailable heat in heat transfer processes. Another mechanism of heat transfer augmentation is the increase of the temperature gradient closed to the wall. As shown in Fig. 5(b), SWLSGs have a structure similar to a deflector, which can guide the central water with high velocity to scour the tube wall. Due to the inertia of the fluid, the boundary layer is in a state of continuous destruction and reconstruction, leading to the increase of the temperature gradient near the tube wall and enhancement of the convective heat transfer between the wall and fluid. Exergy destruction of fluid flow could be divided into two parts. One part is the irreversibility of the fluid due to its viscosity. The other part is converted into the inertia of the fluid to maintain the longitudinal swirling flow.

When the fluid passes through SWLSGs, the fluid obtains tangential velocity and forms symmetrical vortexes due to the pressure difference behind symmetrical wings. It clearly shows the flow characteristics of longitudinal swirling flow with multi-vortexes in Fig. 6(b). The method of swirling strength is adopted to visualize the vortex core region [35] in Fig. 6(c). The vortexes scale near the second insert is significantly larger than that of the first insert. Each time the fluid passes through a symmetrical wing, the strength of vortexes is enhanced and the flow path of the vortex core region becomes longer.

It is obvious that local Nusselt number and friction factor of the enhanced tube are far larger than those of the smooth tube as shown in Fig. 7. The longitudinal swirling flow will be generated or strengthened by each symmetrical wing. The local *Nu* number and *f* fluctuate periodically due to periodical distribution of the symmetric wings of linear array configuration. In a period, the largest *Nu* appears at the rear of the symmetrical wings, where vortexes are generated or strengthened to enhance the mixing of heated and cold fluid. The maximum friction factor occurs on the front surface of symmetric wings, because the frontal impact of the fluid results in a large pressure drop. In addition, the local *Nu* number fluctuates irregularly in the region of the first several symmetri-

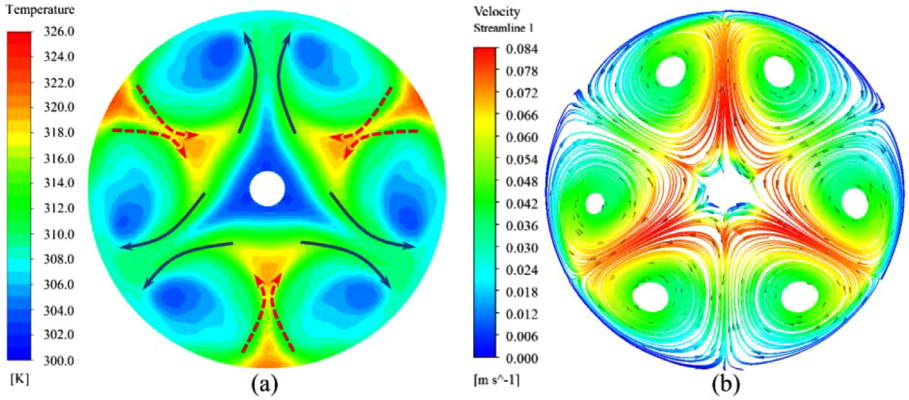

Fig. 5. Temperature contours and streamline: (a) Temperature contours; (b) streamline and velocity distribution.

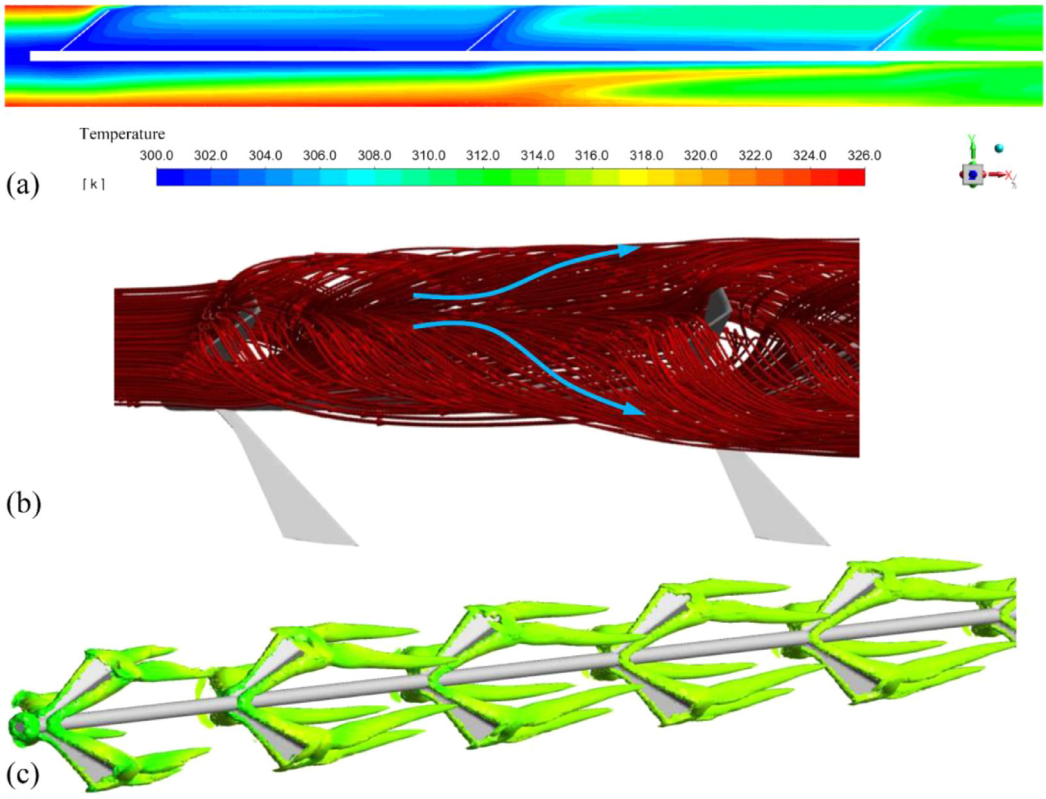

Fig. 6. (a) Temperature contours of vertical section at x = 0–140 mm; (b) Streamlines; (c) Vortex core region by method of swirling strength.

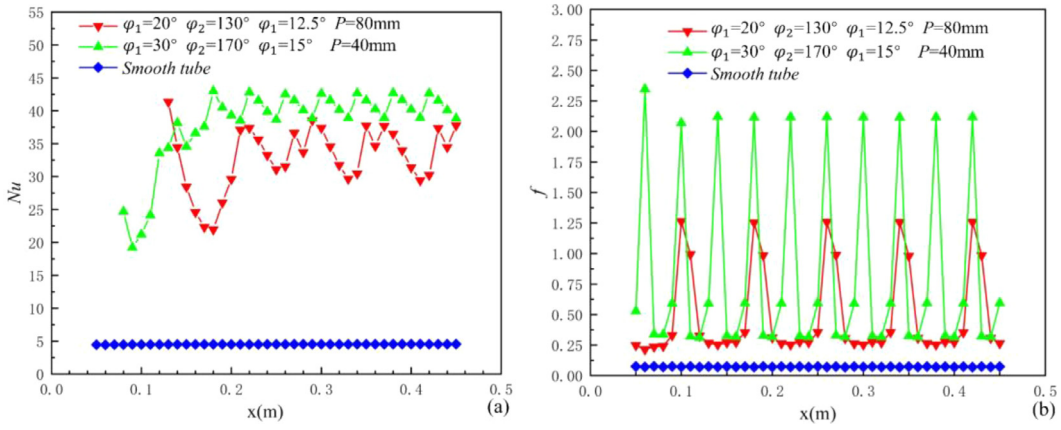

Fig. 7. Local thermal hydraulic performance along the x-axis direction:(a) Nu_x; (b) f_x.

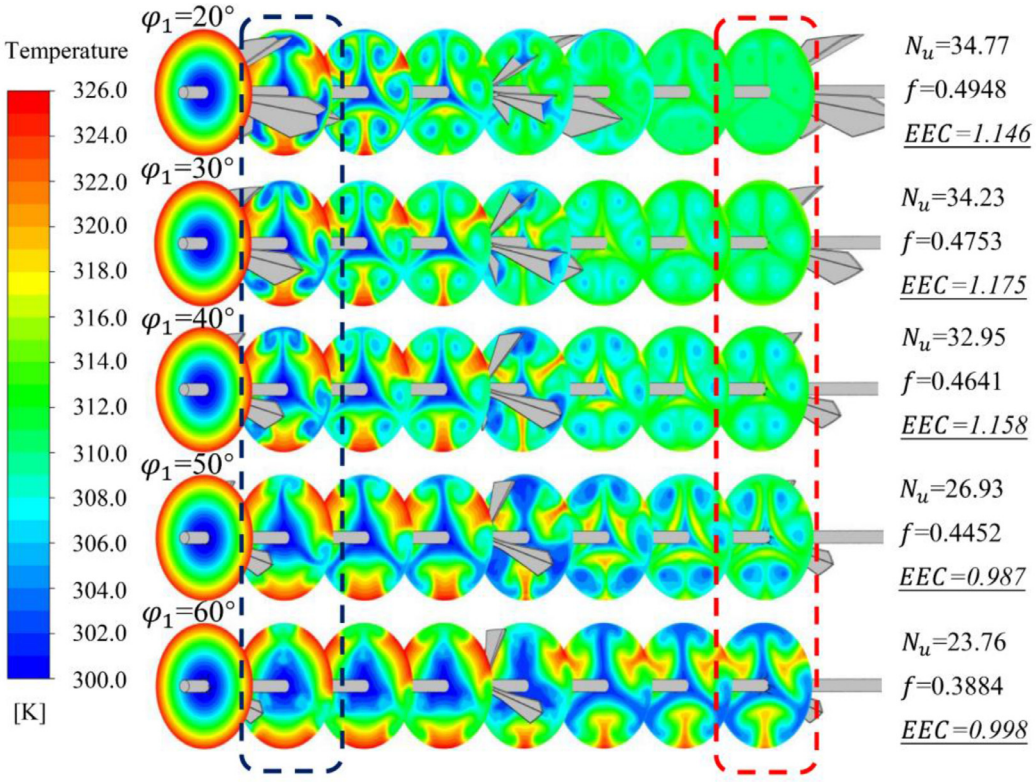

Fig. 8. Temperature contours of different cross sections at the inclined angle of 20–60° with φ_2=110°, φ_3=15° and P = 70 mm.

cal wings that we called it heat transfer transition zone. When the longitudinal swirling flow fully develops, it means that stable heat transfer augmentation is formed. In the fully developed section (about after three symmetrical wings), local *Nu* presents serrated fluctuations with length *x*. Therefore, the heat transfer in the tube is divided into two stages: the transition section and the fully developed section.

4.3. Effect of geometrical parameters

4.3.1. Effect of the inclined angle

The temperature contours of cross sections at the inclined angle of 20–60° with φ_2=110°, φ_3=15° and P = 70 mm are shown in Fig. 8. Due to the constant radial height of symmetrical wings, symmetrical wings have a larger incident flow area as the inclined angle decreases. So that a larger quantity of fluid is guided to scour tube wall, which will compress the high temperature area as shown in the black dotted box. Flow disturbing effect of SWLSGs on the fluid is more significant when the inclined angle φ_1=20°, however, it leads to more fluid momentum loss and increases friction factor and power consumption. After the fluid passes through the first two symmetrical wings, the temperature of the cross-section is almost uniform as shown in the red rectangle. The velocity of fluid scouring the wall is the largest with φ_1=60°, but the incident flow area of symmetrical wings is the smallest. Although the friction factor is the minimum at this time, the temperature uniformity of the fluid after three symmetric wings is still unsatisfactory and *EEC* is less than 1.

4.3.2. Effect of face angle

The cross-section of temperature and velocity distribution with different face angles is x = 45 mm as shown in Fig. 9. In Fig. 9(a), the red circle is the high temperature area formed by the backflow of heated water near the tube wall, which part near the wall also called region of flow deterioration. This is because two adjacent pairs of vortexes collide with each other near the wall, resulting in the loss of fluid momentum and forming the heat transfer deterioration region at a low velocity. When the inclined angle and wing angle are constant, the incident flow area increases with increasing of face angle. Meanwhile, the intensity of the vortex increases enough to breaks the barrier of the adjacent vortices. The flow deterioration area is compressed, so the temperature uniformity of the cross section significantly improved and *Nu* number increased. When the face angle is small, the flow disturbance effect is limited and the intensity of the vortexes is weak, so that the high temperature area still exists. This condition is not conducive to the heat transfer of the fluid, resulting in a low *Nu* number.

As shown in Fig. 9(b), the fluid guided by symmetrical wings has the highest velocity, and the velocity decreases rapidly after the fluid scouring tube wall. The bulges in the blue dotted circle are two high velocity zones formed by the backflow of heated fluid from the tube wall to the center. With the increase of the face angle, the high velocity zone gradually extends to the tube wall in a circular arc to strengthen the multi-vortexes.

4.3.3. Effect of the wing angle

The ratios of exergy destruction of heat transfer and *Nu* varying with different pitches and wing angles are shown in Fig. 10. $E_{xd,\ \Delta T,0}$ is exergy destruction of heat transfer in the smooth tube at a certain Reynolds number. $E_{xd,\ \Delta T,0}$ is fixed when *Re*=900 in simulations. It can be seen that the larger *Nu* ratio, the larger $E_{xd,\ \Delta T,0}/E_{xd,\ \Delta T}$, which means that the exergy destruction of heat transfer in the enhanced tube $E_{xd,\ \Delta T}$ is smaller. Therefore, the overall trend of $E_{xd,\ \Delta T,0}/E_{xd,\ \Delta T}$ and Nu/Nu_0 is consistent. *Nu* number represents the intensity of convection heat transfer, and exergy destruction of heat transfer represents the unavailable heat in heat transfer processes. Therefore, it can be concluded that reducing the unavailable heat can effectively improve the heat transfer capacity of the thermal system. Fig. 11 shows the ratios of ex-

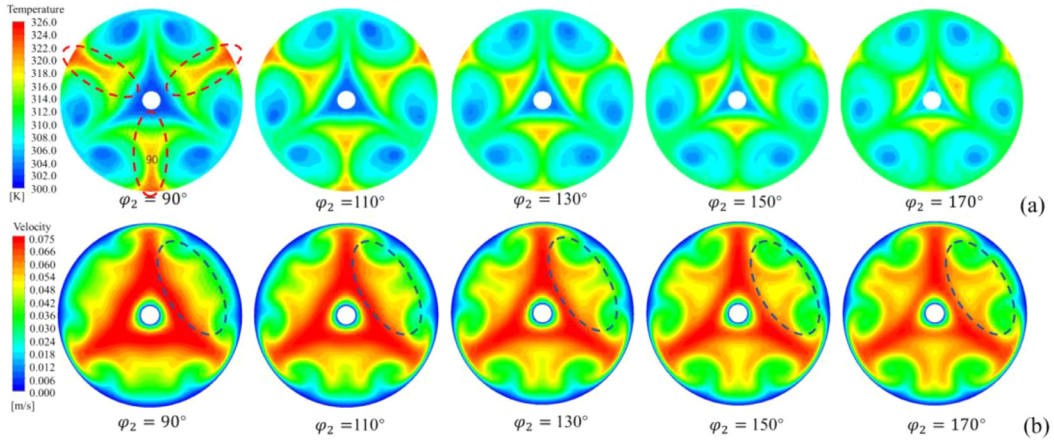

Fig. 9. Cross section at x = 45 mm (φ_1=40°, φ_3=10° and P = 80 mm): (a) temperature contour; (b) velocity distribution.

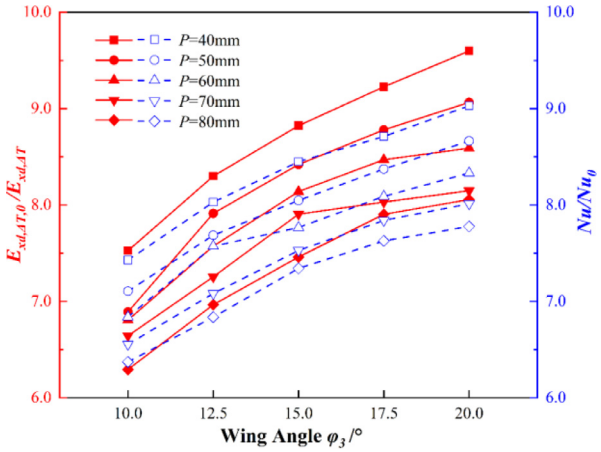

Fig. 10. Variation ratios of exergy destruction of heat transfer and Nusselt number with different pitches and wing angles (φ_1=30° and φ_2=110°).

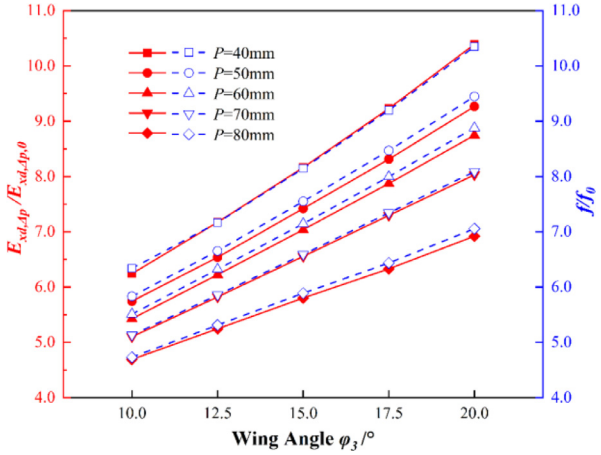

Fig. 11. Variation ratios of exergy destruction of fluid flow and friction factor with different pitches and wing angles.

ergy destruction of fluid flow and friction factor vary with different pitches and wing angles. Since both exergy destruction of fluid flow and friction factor have a direct relationship with the pressure drop in physical meaning and reflect the power consumption, they are almost superposed in numerical results. Nusselt number, flow dissipation and friction factor increase but thermal dissipation decreases with the increasing of wing angle. *EEC* decreases with increase of the wing angle and *EEC* in most cases is greater than 1, which indicates that the heat transfer benefit is greater than the increase of power consumption as shown in Fig. 12.

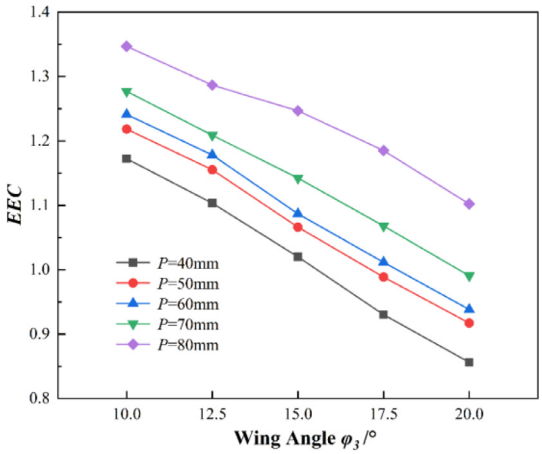

Fig. 12. Variation ratios of *EEC* with different pitches and wing angles.

Fig. 13 illustrates the velocity vector in the cross sections behind symmetrical wings with different wing angles at φ_1=30°, P = 50. It is obvious that the velocity in vortexes is larger and the mixing of fluid is strengthened when the wing angle increases. Increasing the wing angle achieves a similar effect to increasing the symmetric angle, which decreases the area of heat transfer deterioration of low velocity, as shown in the red circle.

4.3.4. Effect of pitch

It is evident that with the increased pitch, both ratio of Nusselt number and fiction factor decrease, while *EEC* increases as shown in Figs. 10 and 11. This is because when the fluid passes through each symmetrical wing, the longitudinal swirling flow is strengthened, and the intensity of the vortexes gradually decreases along with the flow. The times of perturbations per unit length decrease with the increase of pitch, the heat transfer performance weakens and the friction factor decreases. Fig. 14 shows the temperature contours at the axial section in the tube. It can be seen that after three symmetrical wings, the temperature in the tube is basically uniform, so that the enhanced tube with a small pitch will form multi-vortexes in advance and increase the length of the fully developed section. In conclusion, the appropriate pitch should be selected according to different requirements. The inserts with small pitches are suitable for the situation where the heat exchanger

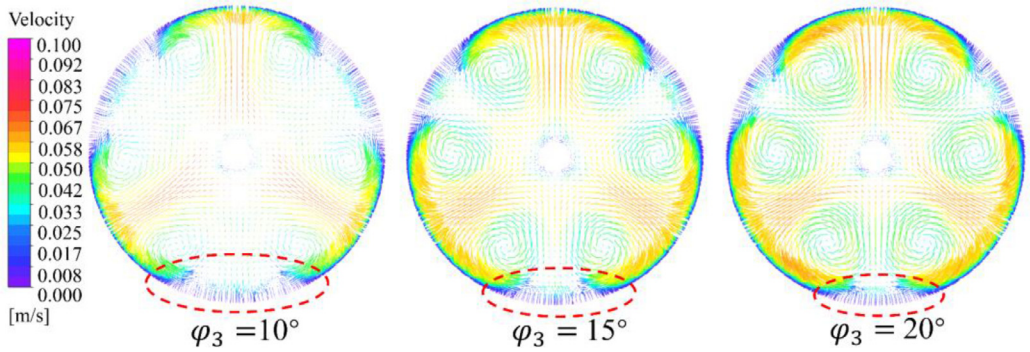

Fig. 13. Comparison of velocity distribution with different wings (P = 50, φ_1=30° and φ_2=110°).

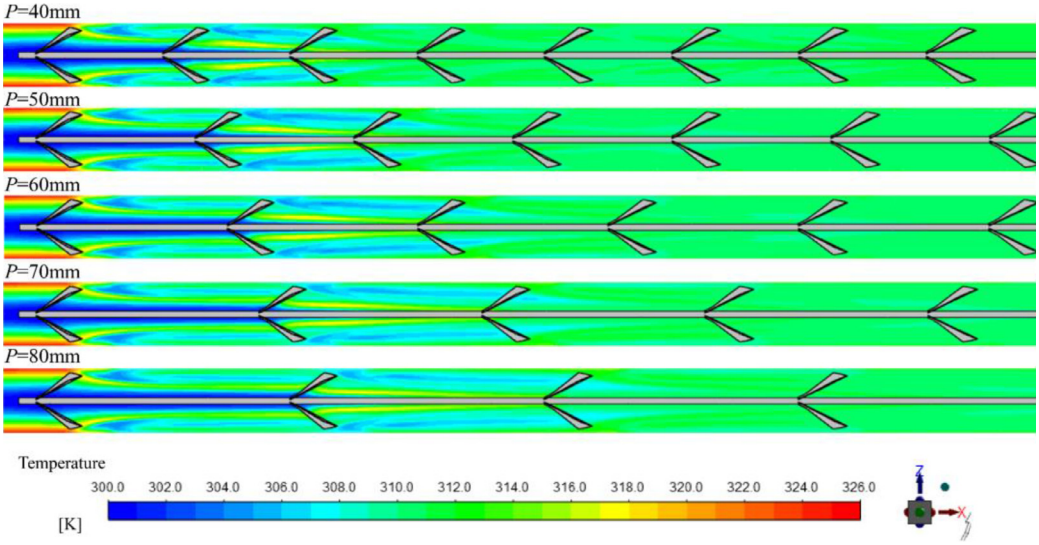

Fig. 14. Comparison of temperature contours of axial cross section with different pitches (φ_1=30°, φ_2=110° and φ_3=12.5°).

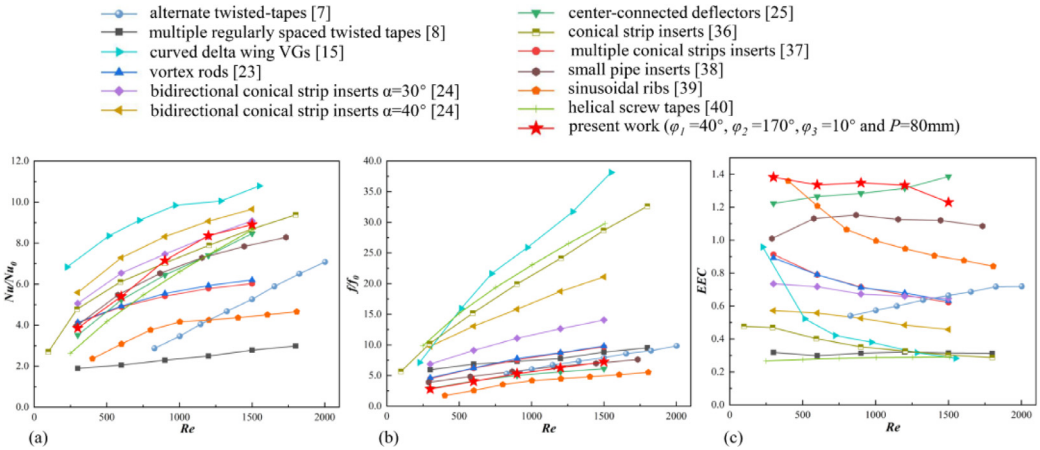

Fig. 15. Comparisons with previous works (a) Nu/Nu_0, (b) f/f_0, (c) EEC value. (φ_1=40°, φ_2=170°, φ_3=10° and P = 80 mm).

tubes are short and lay emphasis on a higher coefficient of heat transfer.

4.4. Comparison with previous works

Fig. 15(a–c) shows the ratio of Nu number, the ratio of friction factor, and the comparison of EEC between the work in this paper and the previous works. Examples include alternate twisted-tapes [7], multiple regularly spaced twisted tapes [8], curved delta wing VGs [15], vortex rods [23], bidirectional conical strip inserts [24], center-connected deflectors [25], conical strip inserts [36], multiple conical strips inserts [37], small pipe inserts [38], sinusoidal ribs [39] and helical screw tapes [40]. Both Nu/Nu_0 and the f/f_0 of SWLSGs increase with the increase of Reynolds number. Nu/Nu_0 of SWLSGs is relatively small at low Reynolds number. However, at high Reynolds numbers (Re = 900–1500), Nu/Nu_0 of SWLSGs is higher than that of most other inserts. And f/f_0 is lower than that of most inserts. This is because the special structure of SWLSGs generates strong longitudinal swirling flow with multi-vortexes while reducing ineffective reverse flow and eddy. There-

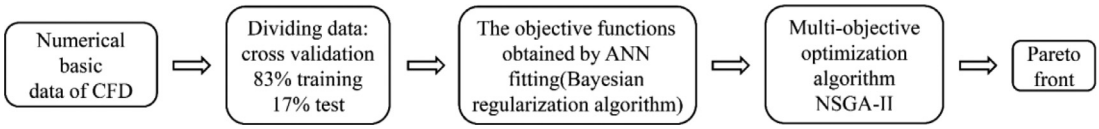

Fig. 16. Optimization procedure of design variables.

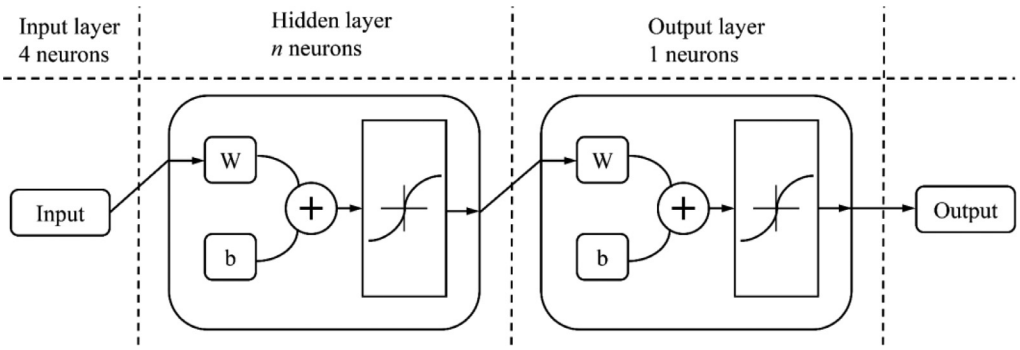

Fig. 17. Neural network structure diagram.

fore, SWLSGs is very effective in improving the comprehensive heat transfer performance in circular tubes under laminar flow.

5. Multi-objective optimization

5.1. Optimization objectives

The numerical investigations are limited, so it is necessary to optimize SWLSGs through the obtained basic data, and finally select the appropriate geometric parameters to achieve the optimal design for different conditions. The ratio of Exergy destruction of fluid flow is adopted as optimization $Objective_1$, representing the power consumption in the tube. When the convective heat transfer becomes more intense, the temperature gradient of the system will be smaller and the exergy destruction of heat transfer decreases. Meanwhile, the exergy destruction of heat transfer represents the unavailable energy of exergy flow, which reflects the utilization efficiency of energy. Therefore, the ratio of exergy destruction of heat transfer is adopted as the optimization $Objective_2$. The minus sign is to minimize the optimization goal. In order to realize efficient heat transfer with low power consumption, considering heat dissipation and power consumption, $Objective_1$ and $Objective_2$ are defined as Eqs. (12) and (13). The ratio of the exergy destruction of heat transfer and fluid flow (*REHF*) is the index to evaluate the benefits and costs of heat exchange.

$$Objective_1 = E_{xd,\Delta p}/E_{xd,\Delta p,0} \tag{12}$$

$$Objective_2 = -E_{xd,\Delta T,0}/E_{xd,\Delta T} \tag{13}$$

$$REHF = \frac{E_{xd,\Delta T,0}/E_{xd,\Delta T}}{E_{xd,\Delta p}/E_{xd,\Delta p,0}} \tag{14}$$

5.2. Optimization procedure

With the $Re = 900$, five different values for inclined angle (φ_1), face angle (φ_2), wing angle (φ_3) and pitch (P) are selected, respectively, and basic data are obtained by CFD numerical simulation. Secondly, a BP neural network with a hidden layer is used to fit the relationship between the input parameters and the output objective function. Furthermore, the trained ANN is selected as the objective function and a non-dominated sorting genetic algorithm (NSGA-II) is used for multi-objective optimization to obtain the Pareto front. Finally, the appropriate design parameters of SWLSGs are selected on the Pareto front according to the engineering requirements. The optimization procedure is shown in Fig. 16 [32,41].

5.3. Fitting of ANN

ANN consists of an input layer, a hidden layer and an output layer as shown in Fig. 17. The number of neurons in the hidden layer plays an important role in the accuracy of the training results of ANN. Therefore, independent verification is required for the number of neurons in the hidden layer. Regression coefficient (*Reg*) and Mean square error (*MSE*) are used as evaluation indexes of the training results. Bayesian regularization algorithm (*B-R*) is applied, and ANN training results $Objective_1$ and $Objective_2$ are shown in Fig. 18. Smaller *MSE* and *REG* closed to 1 have higher fitting accuracy, so hidden layers of 7 and 6 neurons are named $net_{\Delta T}$ and $net_{\Delta p}$, respectively. The comparison between the results of CFD simulation and ANN is shown in Fig. 19. The maximum relative error of $net_{\Delta T}$ is 4.27% and that of $net_{\Delta p}$ is 4.77%. Therefore, ANN has a relatively reliable fitting accuracy.

$$Reg = \sqrt{\frac{\sum_{i=1}^{N}\left(y_{i,ANN}-\bar{y}\right)^2}{\sum_{i=1}^{N}\left(y_i-\bar{y}\right)^2}} \tag{15}$$

$$MSE = \frac{1}{N}\sum_{i=1}^{N}\left(y_i - y_{i,ANN}\right)^2 \tag{16}$$

5.4. Result of optimization

NSGA-II algorithm is used to minimize the two objectives in the commercial software MATLAB, and its specific parameters are as follow: the ranges of the design variables are $\varphi_1 \in [20, 60]$, $\varphi_2 \in [90, 170]$, $\varphi_3 \in [10, 20]$, $P \in [40, 80]$; the population size is 500, the number of iterations is 100, the crossover coefficient is 0.8, the number to population ratio on the Pareto front is 0.15, the functional tolerance is 10^{-4}, and the other parameters are the default values. The Pareto front is obtained as shown in Fig. 20.

According to the properties of the non-dominated solution, if there are multiple optimization objectives, the improvement of any objective function will inevitably weaken other objective functions due to the conflict between the two objectives. Therefore, each

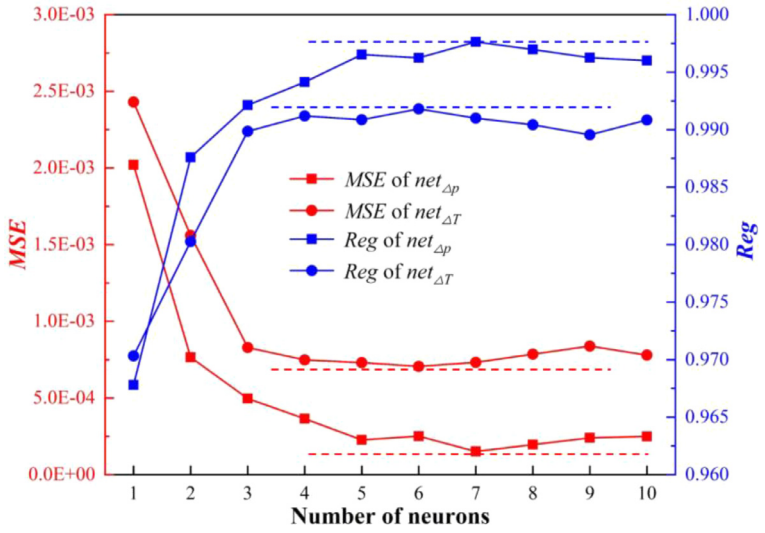

Fig. 18. Neuron independence test.

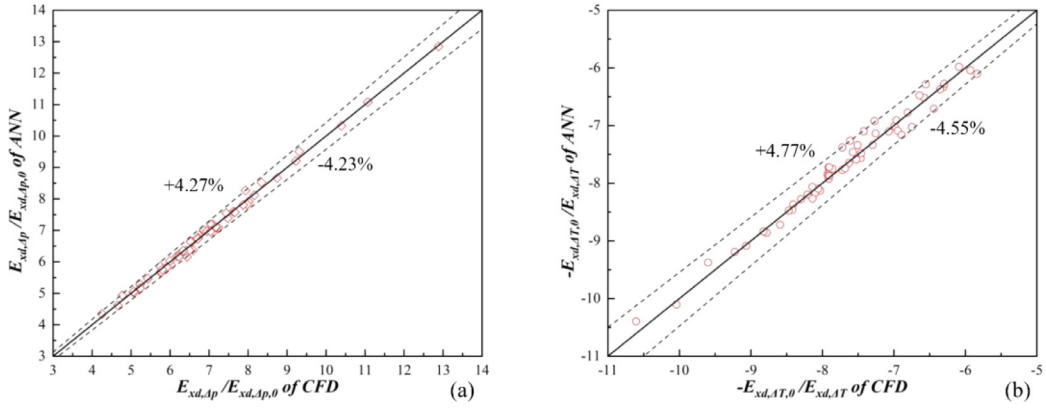

Fig. 19. The relative error of CFD and ANN fitting: (a) $E_{xd,\ \Delta p}/E_{xd,\ \Delta p,\ 0}$; (b) $-E_{xd,\ \Delta T,0}/E_{xd,\ \Delta p}$.

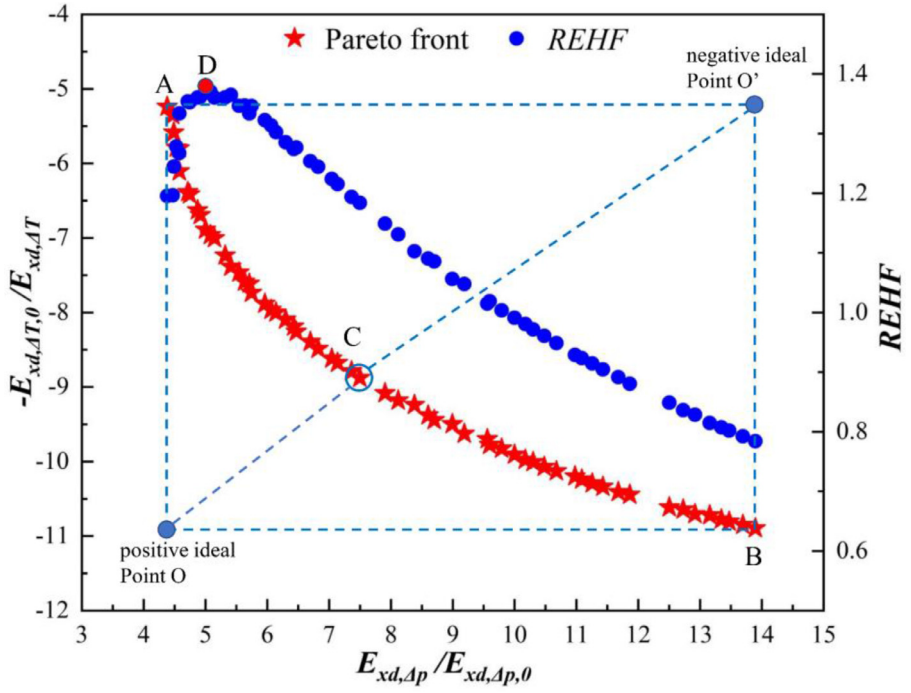

Fig. 20. Pareto front and TOPSIS method result.

point on the Pareto front indicates the minimum exergy destruction of heat transfer will be attained for specific exergy destruction of fluid flow. The points on the Pareto front are all the most advantageous points. For achieving the best synergy between heat transfer and fluid flow, the technique for order preference by similarity to the ideal solution (TOPSIS) is adopted to get point C. We select representative points ABCD on Pareto front for simulation. The errors of these four points between simulated results and predicted results are small: the maximum relative error of exergy destruction of heat transfer is 3.15%, and the maximum relative error of exergy destruction of fluid flow is 3.71%. Therefore, the results of multi-objective optimization in this paper is feasible and convincing. Points A and B are the extreme points, and point C is the optimal point. Point A obtains a low heat transfer coefficient with a low power consumption, and the convection is not sufficient, requiring multiple unit inserts to form the homogeneous temperature characteristic. Point B achieves high heat transfer augmentation with excessive power consumption, so the cost outweighs the benefit. Geometric parameters of SWLSGs at Point C are φ_1=25.6°, φ_2=142.0°, φ_3=13.4° and P = 64.5 mm. Compared with the smooth tube, the exergy destruction of heat transfer decreased 8.88 times, while the exergy destruction of fluid flow increased 7.50 times, *EEC* is 1.26. Point C achieves a high benefit of heat transfer enhancement with moderate power consumption. With the increase of the exergy destruction of fluid flow, *REHF* increases first and then decreases gradually. Point D is the highest point of *REHF*, and the geometric construction of point D is simulated to get *EEC* = 1.476. It can be seen that the optimized enhanced tube has excellent overall heat transfer performance by using the principle of exergy destruction minimization.

6. Conclusion

In this paper, a novel type of inserts, symmetrical wing longitudinal swirl generators, was proposed. SWLSGs had the advantages of simple structure and production, and thermal hydraulic characteristics were numerically investigated under laminar flow. The mechanism of heat transfer enhancement was analyzed, and the following conclusions were obtained.

(1) The mechanisms of heat transfer augmentation of the longitudinal swirl generator were as follow: (i) After each symmetrical wing, the fluid formed the longitudinal swirling flow with multi-vortexes. The formation of each pair vortices would facilitate heated and cold fluid mixing, so as to realize the uniform temperature characteristic in tube. (ii) SWLSGs had a structure similar to a deflector, which guided the cold water in the center to scour the tube wall. Thus, the boundary layer was destroyed due to the inertia of fluid and the temperature gradient near the wall increased.

(2) Orthogonal design of experiment and parametric analysis were applied, the calculation range of various geometric parameters of SWLSGs was φ_1=20–60°, φ_2=90–170°, φ_3=10–20° and P = 40–80 mm. When the Reynolds number was 900, Nusselt number of the enhanced tube was increased by 5.00–10.22 times and the friction factor was increased by 4.05–14.19 times compared with those of the smooth tube. The range of *EEC* was 0.71–1.35. The geometrical parameters with the highest overall heat transfer performance was φ_1=40°, φ_2=170°, φ_3=10° and P = 80 mm.

(3) Both exergy destruction of heat transfer and fluid flow increased with the increasing of face angles and wing angles and the decrease of inclined angles and pitches. Comparing with the smooth tube, the exergy destruction of heat transfer in the enhanced tube decreased by 4.63–11.08 times, while the exergy destruction of fluid flow increased by 3.99–14.00 times.

(4) According to the exergy destruction minimization principle, exergy destruction of heat transfer and fluid flow were taken as two optimization objectives to obtain the neural network fitting function, respectively. NSGA-II was applied to obtain the Pareto front. According to the TOPSIS method, the geometric parameters of compromised point at the Pareto front were φ_1=25.6°, φ_2=142.0°, φ_3=13.4° and P = 64.7 mm, and the *EEC* was 1.26. And the *EEC* of the highest point of *REHF* was 1.476, the excellent overall heat transfer performance was achieved. Therefore, the exergy destruction minimization principle was applied as a criterion to evaluate heat transfer performance.

Declaration of Competing Interest

The authors do not have any possible conflicts of interest.

CRediT authorship contribution statement

Yongji Wang: Conceptualization, Methodology, Software, Validation, Formal analysis, Investigation, Data curation, Writing – original draft, Writing – review & editing, Visualization. **Peng Liu:** Methodology, Software. **Hui Xiao:** Methodology, Software. **Zhichun Liu:** Supervision, Project administration, Funding acquisition. **Wei Liu:** Conceptualization, Writing – review & editing, Supervision, Project administration, Funding acquisition.

Acknowledgment

This work was supported by the National Natural Science Foundation of China (Grant No. 51736004).

Appendix

Since many researchers use *R*3 [42] to evaluate the overall heat transfer performance, we add the analysis content of evaluation index *R*3 for the convenience of other researchers to compare with this study.

$$R3=\frac{Nu_a}{Nu_c} \tag{17}$$

Subscript c is the equivalent value in the smooth tube under the same pressure drop with enhanced tubes.

The method for calculating equivalent Nusselt number is as follows,

$$(Re_a)^3 f_a = (Re_c)^3 f_c \tag{18}$$

Where Re_c is equivalent Reynolds number of the smooth tube.

The inlet boundary conditions are fully developed temperature and velocity. For Re_c < 2100,

$$Nu_c = 4.36 \tag{19}$$

$$f = 64/Re \tag{20}$$

For Re_c > 2100 [43],

$$Nu_c = \frac{(f_c/8)(\mathrm{Re}_c - 1000)Pr}{1 + 12.7\sqrt{f_c/8}\left(\mathrm{Pr}^{2/3} - 1\right)} \tag{21}$$

$$f_c = (0.782 ln Re_c - 1.51)^{-2} \tag{22}$$

When the equivalent Reynolds number is near the critical value between laminar flow and turbulent flow, the turbulent equivalent Reynolds number will be obtained by using laminar friction factor Eq. (20), and the laminar equivalent Reynolds number is obtained by using turbulent friction factor Eq. (22). In these contradictory cases, it is assumed that Re_c can be calculated by the equation of laminar friction factor.

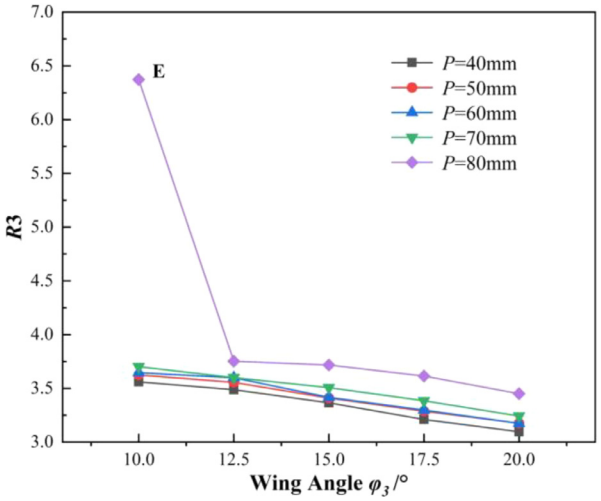

Fig. A.1. Variation ratios of *R*3 with different pitches and wing angles.

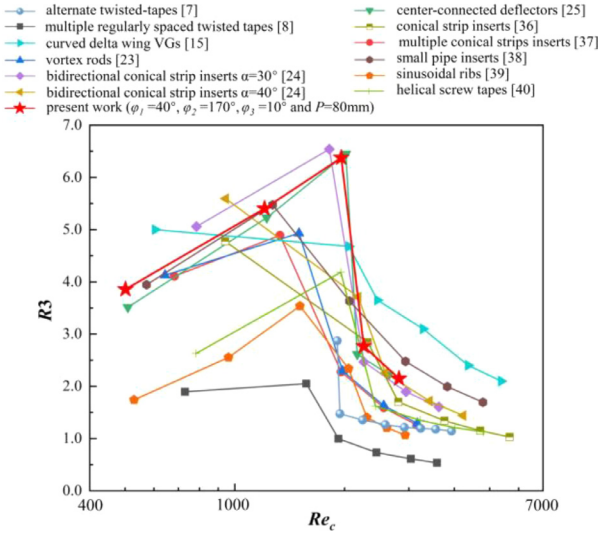

Fig. A.2. Comparisons with previous works.

As most of the simulations in this study is $Re_a = 900$, the equivalent Reynolds number is $Re_c = 1800–4000$ under the strong disturbance of SWLSGs, and this is a transition flow. We have calculated the values of *R*3 for all simulations, which range from 2.79 to 6.37. The equivalent Reynolds numbers of all simulations are larger than 2100 except for point E in Fig. A.1. In smooth tubes, the heat transfer rate of transition flow is much larger than that of laminar flow. As the equivalent Reynolds number of point E is under laminar flow, the equivalent Nusselt number of point E is low. When Re_c is slightly greater than 2100, Nu_c will increase rapidly, resulting in a rapid decline of *R*3 shown in Fig. A.1. The curve trends of *R*3 and *EEC* are consistent, both of which decrease with increasing wing angle and decreasing pitch. Meanwhile, the optimal configuration selected by evaluation indexes of *R*3 and *EEC* is the same. Geometric parameters of the optimal configuration are φ_1=40°, φ_2=170°, φ_3=10° and P = 80 mm, *R*3 of which is 6.37.

Fig. A.2 shows the comparison of *R*3 between previous works and the work in this study. *R*3 of SWLSGs increases as the equivalent Reynolds number increases under laminar flow. $Nu_c = Nu_0 = 4.36$ for $Re_c < 2100$, so the curve of *R*3 is the same as that of Nu/Nu_0. It can be seen that *R*3 decreases rapidly near the critical value of equivalent Reynolds number and decreases with the increase of equivalent Reynolds number under transition flow. On the whole, *R*3 of the optimal configuration in this study is higher than that of most other inserts, so SWLSGs is very effective in improving the comprehensive heat transfer performance in circular tubes under laminar flow.

References

[1] S. Liu, M. Sakr, A comprehensive review on passive heat transfer enhancements in pipe exchangers, Renew. Sustain. Energy Rev. 19 (2013) 64–81, doi:10.1016/j.rser.2012.11.021.

[2] K. Bilen, M. Cetin, H. Gul, T. Balta, The investigation of groove geometry effect on heat transfer for internally grooved tubes, Appl. Therm. Eng. 29 (4) (2009) 753–761, doi:10.1016/j.applthermaleng.2008.04.008.

[3] X.H. Tan, D.S. Zhu, G.Y. Zhou, L.D. Zeng, Heat transfer and pressure drop performance of twisted oval tube heat exchanger, Appl. Therm. Eng. 50 (1) (2013) 374–383, doi:10.1016/j.applthermaleng.2012.06.037.

[4] Y. He, L. Liu, P. Li, L. Ma, Experimental study on heat transfer enhancement characteristics of tube with cross hollow twisted tape inserts, Appl. Therm. Eng. 131 (2018) 743–749, doi:10.1016/j.applthermaleng.2017.12.029.

[5] S. Eiamsa-ard, K. Yongsiri, K. Nanan, C. Thianpong, Heat transfer augmentation by helically twisted tapes as swirl and turbulence promoters, Chem. Eng. Process. 60 (2012) 42–48, doi:10.1016/j.cep.2012.06.001.

[6] Z.M. Lin, L.B. Wang, M. Lin, W. Dang, Y.H. Zhang, Numerical study of the laminar flow and heat transfer characteristics in a tube inserting a twisted tape having parallelogram winglet vortex generators, Appl. Therm. Eng. 115 (2017) 644–658, doi:10.1016/j.applthermaleng.2016.12.142.

[7] K. Wongcharee, S. Eiamsa-ard, Friction and heat transfer characteristics of laminar swirl flow through the round tubes inserted with alternate clockwise and counter-clockwise twisted-tapes, Int. Commun. Heat Mass Transf. 38 (3) (2011) 348–352, doi:10.1016/j.icheatmasstransfer.2010.12.007.

[8] X. Zhang, Z. Liu, W. Liu, Numerical studies on heat transfer and flow characteristics for laminar flow in a tube with multiple regularly spaced twisted tapes, Int. J. Therm. Sci. 58 (2012) 157–167, doi:10.1016/j.ijthermalsci.2012.02.025.

[9] S. Eiamsa-ard, K. Wongcharee, P. Eiamsa-ard, C. Thianpong, Heat transfer enhancement in a tube using delta-winglet twisted tape inserts, Appl. Therm. Eng. 30 (4) (2010) 310–318, doi:10.1016/j.applthermaleng.2009.09.006.

[10] S. Gunes, V. Ozceyhan, O. Buyukalaca, Heat transfer enhancement in a tube with equilateral triangle cross sectioned coiled wire inserts, Exp. Therm. Fluid Sci. 34 (6) (2010) 684–691, doi:10.1016/j.expthermflusci.2009.12.010.

[11] S.W. Chang, K.C. Yu, Heat transfer enhancement by spirally coiled spring inserts with and without segmental solid cords, Exp. Therm. Fluid Sci. 97 (2018) 119–132, doi:10.1016/j.expthermflusci.2018.04.008.

[12] Z. Feng, X. Luo, F. Guo, H. Li, J. Zhang, Numerical investigation on laminar flow and heat transfer in rectangular microchannel heat sink with wire coil inserts, Appl. Therm. Eng. 116 (2017) 597–609, doi:10.1016/j.applthermaleng.2017.01.091.

[13] P. Promvonge, Thermal performance in circular tube fitted with coiled square wires, Energy Convers. Manag. 49 (5) (2008) 980–987, doi:10.1016/j.enconman.2007.10.005.

[14] P.W. Deshmukh, R.P. Vedula, Heat transfer and friction factor characteristics of turbulent flow through a circular tube fitted with vortex generator inserts, Int. J. Heat Mass Transf. 79 (2014) 551–560, doi:10.1016/j.ijheatmasstransfer.2014.08.042.

[15] P.W. Deshmukh, S.V. Prabhu, R.P. Vedula, Heat transfer enhancement for laminar flow in tubes using curved delta wing vortex generator inserts, Appl. Therm. Eng. 106 (2016) 1415–1426, doi:10.1016/j.applthermaleng.2016.06.120.

[16] Q. Chen, M. Wang, N. Pan, Z.Y. Guo, Optimization principles for convective heat transfer, Energy 34 (9) (2009) 1199–1206, doi:10.1016/j.energy.2009.04.034.

[17] W. Liu, H. Jia, Z.C. Liu, H.S. Fang, K. Yang, The approach of minimum heat consumption and its applications in convective heat transfer optimization, Int. J. Heat Mass Transf. 57 (1) (2013) 389–396, doi:10.1016/j.ijheatmasstransfer.2012.10.046.

[18] J. Wang, W. Liu, Z. Liu, The application of exergy destruction minimization in convective heat transfer optimization, Appl. Therm. Eng. 88 (2015) 384–390, doi:10.1016/j.applthermaleng.2014.09.076.

[19] C. Habchi, T. Lemenand, D.D. Valle, H. Peerhossaini, Alternating mixing tabs in multifunctional heat exchanger-reactor, Chem. Eng. Process. 49 (7) (2010) 653–661, doi:10.1016/j.cep.2009.07.003.

[20] N. Zheng, F. Yan, K. Zhang, T. Zhou, Z. Sun, A review on single-phase convective heat transfer enhancement based on multi-longitudinal vortices in heat exchanger tubes, Appl. Therm. Eng. 164 (2020), doi:10.1016/j.applthermaleng.2019.114475.

[21] X.W. Li, H. Yan, J.A. Meng, Z.X. Li, Visualization of longitudinal vortex flow in an enhanced heat transfer tube, Exp. Therm. Fluid Sci. 31 (6) (2007) 601–608, doi:10.1016/j.expthermflusci.2006.06.007.

[22] X.W. Li, J.A. Meng, Z.Y. Guo, Turbulent flow and heat transfer in discrete double inclined ribs tube, Int. J. Heat Mass Transf. 52 (3–4) (2009) 962–970, doi:10.1016/j.ijheatmasstransfer.2008.07.027.

[23] N. Zheng, P. Liu, F. Shan, J. Liu, Z. Liu, W. Liu, Numerical studies on thermo-hydraulic characteristics of laminar flow in a heat exchanger tube fitted with vortex rods, Int. J. Therm. Sci. 100 (2016) 448–456, doi:10.1016/j.ijthermalsci.2015.09.008.

[24] P. Liu, N. Zheng, F. Shan, Z. Liu, W. Liu, Heat transfer enhancement for laminar flow in a tube using bidirectional conical strip inserts, Int. J. Heat Mass Transf. 127 (2018) 1064–1076, doi:10.1016/j.ijheatmasstransfer.2018.07.128.

[25] J.Y. Lv, Z.C. Liu, W. Liu, Active design for the tube insert of center-connected deflectors based on the principle of exergy destruction minimization, Int. J. Heat Mass Transf. 150 (2020) 119260, doi:10.1016/j.ijheatmasstransfer.2019.119260.
[26] A. Bejan, A study of entropy generation in fundamental convective heat transfer, J. Heat Transf. 101 (4) (1979) 718, doi:10.1115/1.3451063.
[27] A. Bejan, Entropy generation minimization: the new thermodynamics of finite-size devices and finite-time processes, J. Appl. Phys. 79 (3) (1996) 1191–1218, doi:10.1063/1.362674.
[28] Z.Y. Guo, H.Y. Zhu, X.G. Liang, Entransy—a physical quantity describing heat transfer ability, Int. J. Heat Mass Transf. 50 (13–14) (2007) 2545–2556, doi:10.1016/j.ijheatmasstransfer.2006.11.034.
[29] Q. Chen, X.G. Liang, Z.Y. Guo, Entransy theory for the optimization of heat transfer – a review and update, Int. J. Heat Mass Transf. 63 (2013) 65–81, doi:10.1016/j.ijheatmasstransfer.2013.03.019.
[30] W. Liu, P. Liu, J.B. Wang, N.B. Zheng, Z.C. Liu, Exergy destruction minimization: a principle to convective heat transfer enhancement, Int. J. Heat Mass Transf. 122 (2018) 11–21, doi:10.1016/j.ijheatmasstransfer.2018.01.048.
[31] B. Minasny, A.B. Mcbratney, The neuro-m method for fitting neural network parametric pedotransfer functions, Soil Sci. Soc. Am. J. 66 (2) (2002) 352–361, doi:10.2136/sssaj2002.0352.
[32] T. Cong, G. Su, S. Qiu, W. Tian, Applications of ANNs in flow and heat transfer problems in nuclear engineering: a review work, Prog. Nucl. Energy 62 (2013) 54–71, doi:10.1016/j.pnucene.2012.09.003.
[33] K. Deb, A. Pratap, S. Agarwal, T. Meyarivan, A fast and elitist multiobjective genetic algorithm: NSGA-II, IEEE Trans. Evol. Comput. 6 (2) (2002) 182–197, doi:10.1109/4235.996017.
[34] C.W. Reynolds, Heat transfer to fully developed laminar flow in a circular tube with arbitrary circumferential heat flux, J. Heat Transf. 82 (2) (1960) 108, doi:10.1115/1.3679887.
[35] J. Zhou, R.J. Adrian, S. Balachandar, T.M. Kendall, Mechanisms for generating coherent packets of hairpin vortices in channel flow, J. Fluid Mech. 387 (1999) 353–396, doi:10.1063/1.4933250.
[36] Y. You, A. Fan, W. Liu, S. Huang, Thermo-hydraulic characteristics of laminar flow in an enhanced tube with conical strip inserts, Int. J. Therm. Sci. 61 (2012) 28–37, doi:10.1016/j.ijthermalsci.2012.06.013.
[37] P. Liu, N. Zheng, F. Shan, Z. Liu, W. Liu, An experimental and numerical study on the laminar heat transfer and flow characteristics of a circular tube fitted with multiple conical strips inserts, Int. J. Heat Mass Transf. 117 (2018) 691–709, doi:10.1016/j.ijheatmasstransfer.2017.10.035.
[38] W. Tu, Y. Tang, J. Hu, Q. Wang, L. Lu, Heat transfer and friction characteristics of laminar flow through a circular tube with small pipe inserts, Int. J. Therm. Sci. 96 (2015) 94–101, doi:10.1016/j.ijthermalsci.2015.04.013.
[39] J. Du, Y. Hong, S.M. Huang, W.B. Ye, S. Wang, Laminar thermal and fluid flow characteristics in tubes with sinusoidal ribs, Int. J. Heat Mass Transf. 120 (2018) 635–651, doi:10.1016/j.ijheatmasstransfer.2017.12.047.
[40] P. Sivashanmugam, S. Suresh, Experimental studies on heat transfer and friction factor characteristics of laminar flow through a circular tube fitted with helical screw-tape inserts, Appl. Therm. Eng. 26 (16) (2006) 1990–1997, doi:10.1016/j.applthermaleng.2006.01.008.
[41] A. Abdollahi, M. Shams, Optimization of shape and angle of attack of winglet vortex generator in a rectangular channel for heat transfer enhancement, Appl. Therm. Eng. 81 (2015) 376–387, doi:10.1016/j.applthermaleng.2015.01.044.
[42] R.M. Manglik, A.E. Bergles, Swirl flow heat transfer and pressure drop with twisted-tape inserts, Adv. Heat Transf. 36 (02) (2003) 183–266, doi:10.1016/S0065-2717(02)80007-7.
[43] V. Gnielinski, New equations for heat and mass transfer in turbulent pipe and channel flows, Int. J. Chem. Eng. 16 (1976) 359–368.